



This is the accepted manuscript made available via CHORUS. The article has been published as:

# Nonlinear optical control of chiral charge pumping in a topological Weyl semimetal

M. Mehdi Jadidi, Mehdi Kargarian, Martin Mittendorff, Yigit Aytac, Bing Shen, Jacob C. König-Otto, Stephan Winnerl, Ni Ni, Alexander L. Gaeta, Thomas E. Murphy, and H. Dennis Drew

Phys. Rev. B **102**, 245123 — Published 16 December 2020

DOI: 10.1103/PhysRevB.102.245123

## Nonlinear Optical Control of Chiral Charge Pumping in a Topological Weyl Semimetal

M. Mehdi Jadidi,<sup>1,\*</sup> Mehdi Kargarian,<sup>2,†</sup> Martin Mittendorff,<sup>3,4</sup> Yigit Aytac,<sup>3,5</sup> Bing Shen,<sup>6</sup> Jacob C. König-Otto,<sup>7</sup> Stephan Winnerl,<sup>7</sup> Ni Ni,<sup>6</sup> Alexander L. Gaeta,<sup>1</sup> Thomas E. Murphy,<sup>3</sup> and H. Dennis Drew<sup>8,‡</sup>

Solids with topologically robust electronic states exhibit unusual electronic and optical transport properties that do not exist in other materials. A particularly interesting example is chiral charge pumping, the so-called chiral anomaly, in recently discovered topological Weyl semimetals, where simultaneous application of parallel DC electric and magnetic fields creates an imbalance in the number of carriers of opposite topological charge (chirality). Here, using time-resolved terahertz measurements on the Weyl semimetal TaAs in a magnetic field, we optically interrogate the chiral anomaly by dynamically pumping the chiral charges and monitoring their subsequent relaxation of the non-equilibrium state. Theory based on Boltzmann transport shows that the observed effects originate from an optical nonlinearity in the chiral charge pumping process. Our measurements reveal that the non-equilibrium chiral excitation relaxation time is much greater than 1 ns. The observation of terahertz-controlled chiral carriers with long coherence times and topological protection suggests the application of Weyl semimetals for quantum optoelectronic technology.

#### I. INTRODUCTION

The control of quantum matter with light is at the forefront of condensed matter physics research. Recently, strong optical pumping has been employed to generate exotic electronic states in solids, not present at equilibrium, such as light-induced superconductivity<sup>1</sup>, nonlinear Hall effect<sup>2</sup>, and ultrafast symmetry switch<sup>3</sup>. Among the recently discovered solids, Weyl semimetals have attracted attention because they are predicted to exhibit a host of novel topological properties not seen in other materials<sup>4-6</sup> due to the Berry curvature of the Weyl nodes. An example of a topological Weyl fermions transport effect is the chiral anomaly, where simultaneous application of parallel static electric and magnetic fields pumps the carriers from one Weyl node to the other, unbalancing the number of chiral carriers<sup>7,8</sup>. Since the Weyl nodes of oppsite chirality are separated in momentum space, the relaxation of chiral anomaly is expected to be slow, similar to long intervalley scattering of carriers in 2D semiconductors<sup>9</sup>. Recently, terahertz-excited Weyl fermions via chiral anomaly in a Weyl semimetal were proposed as an attractive platform for qubits with large coherence time to gate time ratio 10. While terahertz excitation of chiral charge pumping has been observed in TaAs<sup>11</sup>, the chiral population relaxation time in a Weyl semimetal have yet to be measured.

Here we demonstrate optical (at terahertz frequencies) excitation and control of chiral charge pumping. We employ terahertz pump-probe measurements in a magnetic field on the Weyl semimetal tantalum arsenide (TaAs) to optically modify the dynamical chiral charge pumping and monitor its subsequent relaxation. In these measurements, a strong quasi-continous wave pulse (pump) at 3.4 THz (14 meV) polarized parallel to an applied magnetic field modifies the

chiral current. The change in the chiral current is monitored via reflection measurement of a second, co-polarized weak pulse (probe) at the same photon energy as pump as a function of the time delay between the two pulses. In addition to the expected fast response of hot carrier relaxation, we observe a metastable response (>> 1 ns) that we associate with the pump-induced change in the dynamical chiral current leading to extraordinarily long lived nonequilibrium states. Our study of the chiral charge pumping circumvents<sup>11</sup> the problems arising from electrical contacts and current jetting that have plagued electrical magnetoresistance measurements<sup>12,13</sup>. Also, by using low-energy photons in the terahertz domain, we ensure that only carriers near the Weyl pockets are excited and studied- a condition that has not been met in prior experimental studies reported to  $date^{14-17}$ .

Our measurements at different magnetic fields, pump fluences, and pump polarizations disentangle the chiral charge pumping signals from the pump-induced transient hot carriers effects. Our results demonstrate the ability to optically control the dynamical chiral charge pumping. While there is no static current produced by the pump pulse, it creates correlated excitations (or quasi-particles) in the opposing Weyl nodes that persist long after the pump pulse has passed. In addition to the chiral population relaxation time, these experiments yield the electron cooling rate as a function of magnetic field and polarization in TaAs, which varies widely due to phase space restrictions for scattering between Landau levels. We present a theory, based on the Boltzmann transport equations in the presence of a strong driving optical field, that explains the observed slow relaxation rate.

The paper is organized as follows. In Sec.II we introduce the concept and theoretical predictions of dynamical chiral

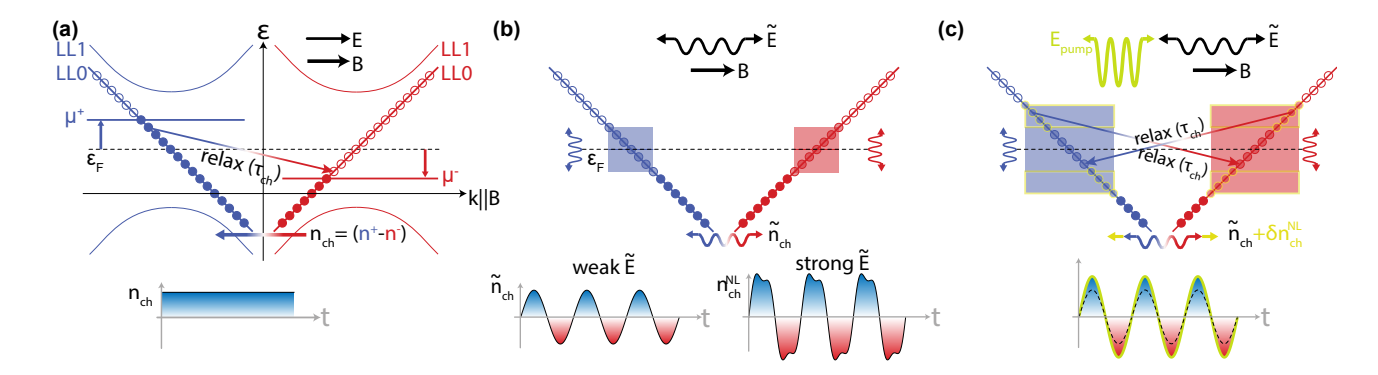


FIG. 1. (a) Static charge pumping of chiral carriers in the zeroth Landau level. Red and blue colors denote different chiralities of carriers. The chiral charge imbalance relaxes back to equilibrium with a time constant of  $\tau_{\rm ch}$ . (b) Dynamical charge pumping, shaded blue and red regions around Fermi level  $\epsilon_F$ , are produced by an oscillating optical field polarized parallel to B. For strong optical excitation, the chiral charge oscillation between the Weyl nodes becomes nonlinear in  $\tilde{E}$  leading to anharmonic oscillation of chiral charges. (c) Strong optical field  $\tilde{E}_{\text{pump}}$  enhances the chiral current generated by  $\tilde{E}||B|$ . When  $\tilde{E}_{\text{pump}}$  is turned off, the extra pump-induced chiral carrier distribution (illustrated by a yellow border) slowly relaxes back via inter-Weyl-node relaxation.

response. The experimenta pump-probe setup is introduced in Sec.III. The results at zero magnetic field is discussed in Sec.IV, and the dynamical chiral charge pumping measurements are presented in Sec.V, and the polarization dependece is discussed in Sec.VI. We summarize our findings in Sec.VII. Details of theory and some complementary measurements are relegated to accompanying Supplemental Materials (SM).

#### II. CONCEPT AND THEORY

The chiral charge pumping process leads to negative DC magneto-resistance, decrease of resistance in the presence of an applied parallel magnetic field, that is unusual among conventional metals/semimetals. The observation of negative DC magneto-resistance in Wevl semiemetals was initially thought to be a conclusive experimental signature of the chiral anomaly<sup>13,18</sup>. However, it was later found that other classical effects can give rise to similar effect in semimetals, making it challenging for electrical measurements to discriminate the chiral anomaly from other effects such as current jetting<sup>12,19</sup>. The relaxation time of the chiral imbalance in the Weyl semimetal TaAs was indirectly extracted and estimated to be tens of picoseconds from negative magneto-resistance measurements despite current jetting effects<sup>13</sup>. However, the relaxation of unbalanced chiral Weyl carriers requires large momentum scattering and is theoretically expected to be much slower<sup>20</sup>.

We consider extreme quantum limit where only the chiral Landau levels (LL0s) are occupied. At equilibrium, the two LL0s host equal number of left- and right-moving chiral carriers along the magnetic field. The static chiral charge pumping scheme is illustrated in Fig. 1(a), where the application of parallel static electric  $\bf E$  and magnetic  $\bf B$  fields unbalances the chemical potentials in the two LL0s with opposite chirality ( $\mu^+$  and  $\mu^-$ ), relaxing back to equilibrium with the chiral charge relaxation time  $\tau_{\rm ch}$ .

The chiral charge pumping can also be realized dynam-

ically where, instead of constant chiral charge imbalance around the two Weyl nodes, their chemical potentials oscillate antisymmetrically around the equilibrium Fermi energy  $^{11}$ . As illustrated in Fig. 1(b), dynamical chiral charge pumping can be achieved by applying an oscillatory optical field of  $\mathbf{E}(t)$  at frequency of  $\omega$  parallel to a static  $\mathbf{B}$  field. In this case, the chiral carriers oscillate in between the two nodes synchronously with  $\mathbf{E}(t)$ , leading to quasiparticle excitations near the chemical potential energy, illustrated by shaded blue and red regions in Fig. 1(b). The density of the quasiparticles generated by dynamical chiral charge pumping is  $\tilde{n}_{\rm ch}(\omega)/2$  in each Weyl node, where  $\tilde{n}_{\rm ch}(\omega)$  is the amplitude of the oscillatory chiral charge imbalance,

$$|\tilde{n}_{\rm ch}(\omega)| = |n_+ - n_-| = \frac{2e^2}{h^2} \frac{\tau_{ch}}{\sqrt{1 + \omega^2 \tau_{ch}^2}} \left| \tilde{\mathbf{E}}(\omega) \cdot \mathbf{B} \right| \quad (1)$$

with  $n_+$  and  $n_-$  as densities of carriers with opposite chirality, and  $\tilde{\mathbf{E}}(\omega)$  is the complex amplitude of the oscillating field. The associated magneto-optical conductivity is (see Sec.III in SM<sup>21</sup>),

$$\sigma_{\rm ch}(\omega) = \frac{e^3 v}{h^2} \frac{\tau_{ch}}{1 - i\omega \tau_{ch}} B \approx i \frac{e^3 v}{h^2 \omega} B \tag{2}$$

where v is the Fermi velocity, and we have assumed  $\omega \tau_{\rm ch} \gg 1$  in the second equality. We note that the dynamical chiral charge pumping scheme is only observable for excitations created by low-energy photons where the Weyl carriers with opposite chirality exist. For TaAs, this condition limits the photon energy to  $\hbar\omega < 50$  meV (12 THz)<sup>22,23</sup>. In the limit of  $\omega \to 0$ , (1) and (2) reproduce the chiral charge imbalance and DC magneto-conductivity<sup>24</sup>.

We consider the case where  $\mathbf{E}(\omega)$  is sufficiently intense so that the resulting  $\tilde{n}_{ch}$  becomes a nonlinear function of the excitation field  $\tilde{\mathbf{E}}(\omega)$ , similar to anharmonic oscillation of an oscillator under a strong driving force. This nonlinear scheme is illustrated in the lower right part of Fig. 1(b). We note that

nonlinear optical response of Weyl semimetals has been recently explored through measurements of second harmonic generation  $^{14}$  and the circular photogalvanic effect  $^{15-17,25}$ . In our study, we specifically explore how a strong optical pump  $\tilde{\mathbf{E}}_{pump}$  can modify and control the chiral charge pumping conductivity by driving it to the nonlinear regime. As illustrated in Fig. 1c, the strong optical pump  $\tilde{\mathbf{E}}_{pump}$  enhances the quasiparticle density produced by dynamical chiral charge pumping in (1). The enhancement is calculated as (see Sec.III in SM $^{21}$  for details of derivation)

$$\delta \tilde{n}_{\rm ch}(\omega) = \frac{15\alpha^2 e^4 v^2}{4h^2 \omega^4 \tau} \left( \frac{\tilde{\mathbf{E}}_{\rm pump} \cdot \mathbf{B}}{B} \right)^2 \tilde{\mathbf{E}} \cdot \mathbf{B}, \tag{3}$$

where  $\alpha \equiv 2/mv^2$  and m is the mass associated with the finite Lifshitz transition energy of the Weyl bands which is the origin of the nonlinearity. The nonlinear contribution  $\delta\sigma_{\rm ch}^{\rm NL}$  to the chiral charge pumping conductivity can be written as  $\sigma_{\rm ch}\left(\omega, \tilde{E}_{\rm pump}(\omega)\right) = \sigma_{\rm ch}(\omega) + \delta\sigma_{\rm ch}^{\rm NL}$ , where

$$\delta\sigma_{\rm ch}^{\rm NL} = i \frac{9\alpha^2 e^5 v^3}{8h^2 \omega^3} \left( \frac{\tilde{\mathbf{E}}_{\rm pump} \cdot \mathbf{B}}{B} \right)^2 B, \tag{4}$$

which exhibits a linear dependence on B similar to the linear conductivity in (2).

The nonlinear process described by equations (3) and (4) predicts that the chiral current can be optically enhanced as shown in Fig. 1c. Furthermore, by driving the chiral charge pumping to the nonlinear regime and observing the relaxation dynamics in the time domain, one can measure the chiral charge relaxation with time constant  $\tau_{ch}$ , i.e. how long it takes for the excited carriers in the chiral Landau level to relax back to the equilibrium chemical potential. Since  $\tau_{ch}$  is expected to be long, the optical modification of chiral current will be longlived. Assuming parameters for TaAs and optical pumping with field strength of 50 kV/cm (achievable in our pulsed THz pumping experiments; see Sec.V in SM<sup>21</sup>),  $\delta \sigma_{\rm ch}^{\rm NL}/\sigma_{\rm ch} \approx 1$ , suggesting the optical pumping can fully modify the chiral charge pumping process. We note that the long-lived optical control of chiral charge pumping described by equations (3) and (4) is relevant only in the quantum limit where the carriers occupy only the zeroth Landau level LLO. In the semiclassical regime the pump-excited chiral carriers can relax back to equilibrium by inter-Landau level scattering within each Weyl node.

## III. EXPERIMENTAL SETUP

The Weyl semimetal considered in our study is tantalum arsenide (TaAs). Single crystals of TaAs were grown using the chemical vapor transport method with iodine as the transport agent<sup>16</sup>. Unlike the other discovered Weyl semiemtals, TaAs has a Fermi energy very close to the Weyl nodes in the linear regime of the bands, so that the electrons at the Fermi surface behave like massless chiral Weyl fermions<sup>22,23,26,27</sup>. This

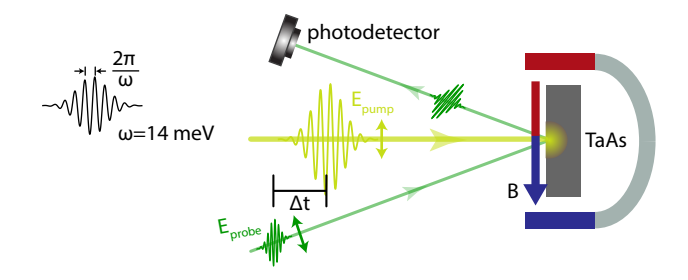


FIG. 2. The pump-probe setup at the photon energy of  $\hbar\omega=14$  meV in reflection geometry. Both pulses are co-polarized to the (001) face of TaAs crystal that is placed inside a magnet.

makes TaAs especially attractive for studies of Weyl fermions interactions with light.

TaAs has two types of Weyl nodes namely W1 (4 pairs) and W2 (8 pairs), where W2 nodes are closer to the chemical potential than W1 by about 12 meV<sup>23</sup>. We estimate that for  $B \ge 2$  T, the W2 Weyl nodes are in the extreme quantum limit, whereas W1 carriers are always in the semiclassical regime occupying few Landau levels as discussed in Sec.VD in SM<sup>21</sup>. In TaAs, for ( $\geq$  50 meV) energies, the pairs of Weyl bands merge into single bands, causing Weyl bands and Weyl fermions to exist only at low energy excitations<sup>22,23</sup>. Also, other than W1 and W2 Weyl bands, the chemical potential crosses a non-Weyl band with a band gap of  $\leq 50 \text{ meV}^{22,23,28}$ . Therefore, in order to probe the dynamics of Weyl fermions in TaAs, photon energy below 50 meV is required. To probe the idea of nonlinear optical control of chiral charge pumping and measure the chiral population relaxation time  $\tau_{ch}$ , we design pump-probe experiments at low photon energy (terahertz) in a magnetic field on TaAs as shown in Fig. 2. All the pumpprobe measurements were carried out using quasi-continuous wave pulses at a photon energy of 14 meV ( $\equiv$  3.4 THz), which is well inside the Weyl bands where only the Weyl fermions with opposite chirality are excited<sup>22,23</sup>. Furthermore, at 14 meV, the photons do not have enough energy to excite additional carriers in the non-topological bands<sup>22</sup>.

The TaAs crystal is mounted inside a magnet with a magnetic field parallel to the ab plane of the crystal. An intense pump pulse polarized parallel to applied magnetic field ( $\mathbf{E}_{pump} \parallel \mathbf{B}$ ) drives the chiral charge pumping process to the nonlinear regime. In order to monitor the pump-induced change in the conductivity, the reflection change of a weak probe pulse ( $\mathbf{E}_{probe} \parallel \mathbf{B}$ ), i.e.  $\Delta R/R$ , is measured as a function of the time delay between the pump and probe pulses. We carry out measurements at different magnetic fields, pump fluences, and pump polarizations.

In the presented pump-probe measurements on TaAs, the bulk response is mainly being excited and monitored, as the admittance associated with the surface response is very small compared with the high index of refraction of TaAs at 14 meV. Equations (3) and (4) predict pump-induced increase in the quasiparticle density and conductivity. According to (3) and (4), the signature of pump-induced nonlinearity in the chiral charge pumping is a long-lived positive change in the probe reflection. We note that other nonlinearities are present, such

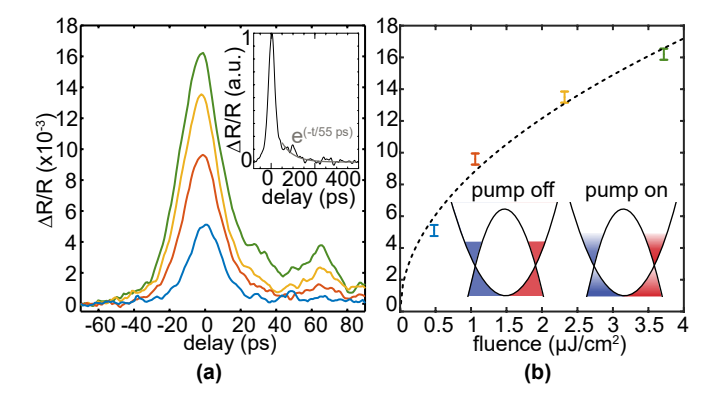


FIG. 3. Pump-probe at B=0. (a) Fractional pump-induced increase in probe reflection for variety of pump fluences as a function of pump-probe time delay. Pump-probe traces exhibit two relaxation time constants of <15 ps (pulsewidth-limited) and  $\approx$ 55 ps, as shown in the inset. (b) Maximum change (occurs at zero time delay) in probe reflection as a function of pump fluence extracted from part (a). The dashed curve is a power-law fit exhibiting square-root dependence of the peak value on the pump fluence, consistent with the pump-induced hot carriers in the Weyl bands.

as hot carriers effects, that can contribute to a pump-induced change in the probe reflection. To distinguish those, we carry out measurements at different magnetic fields, pump fluences, and pump polarizations. Furthermore, since the nonlinearities have different time scales, the time delay scan helps us differentiate various pump-induced nonlinearities.

# IV. PUMP-PROBE MEASUREMENTS AT ZERO MAGNETIC FIELD

We present the pump-probe results at zero magnetic field and conclude that the response is attributed to the pump-induced hot carriers in TaAs. Fig. 3 shows the pump-probe measurement results without an applied magnetic field. In Fig. 3(a), the measured relative pump-induced change in the probe reflection is plotted as a function of pump-probe time delay for variety of pump fluences. We observe a positive change in probe reflection that increases with the pump fluence. The probe reflection relaxes immediately back to its equilibrium level through a fast process that cannot be resolved by the pulsewidth used here followed by a slower relaxation tail. The slower relaxation process can be fit to an exponential function with a time constant of 55 ps, as shown by the grey curve in the inset of Fig. 3(a).

The zero magnetic field results in Fig. 3(a) can be understood by the effect of carrier heating in the Weyl bands of TaAs. The pump pulse heats up the carriers in the Weyl bands to a temperature T higher than the initial lattice temperature (10 K). This process leads to the excitation of hot carriers around the Weyl nodes, which elevates the Drude weight by an amount proportional to  $T^2$  in a 3D Dirac/Weyl semimetal<sup>5</sup>. The reflection, which is linearly proportional to the Drude weight, will also increase by  $\Delta R \propto T^2$ . We note that the quadratic increase of reflection with temperature has

been previously observed in TaAs<sup>29</sup> and other 3D Dirac/Weyl semimetals<sup>30</sup>. From the temperature dependence of the linear reflection data in TaAs<sup>29</sup>, we estimate the pump-induced carrier temperature rise to be around 50 K for the highest pump fluence considered here. After the pump pulse, the carriers start to cool down via phonon emissions, and the increased reflection relaxes back to the equilibrium value. Thus, the two relaxation time constants of  $\ll 30$  ps and 55 ps are related to the electron-phonon relaxation times. Since both the photon energy (14 meV) and the thermal energy associated with the carrier temperature rise are below the energy of optical phonons in TaAs, the hot carrier relaxation will occur through acoustic phonons<sup>31</sup>. A possible scenario for electron-phonon relaxation observed in our experiments is that the faster process is a disorder-assisted electron-phonon relaxation process, whereas the slower one is related to conventional electronacoustic phonon collisions<sup>31</sup>. We note that in graphene, as another Dirac semimetal, similar processes govern the hot carrier relaxations<sup>32,33</sup> and pump-probe dynamics<sup>34,35</sup>. For disorder-assisted electron-phonon cooling in 3D Dirac/Weyl semimetals, the carrier temperature rise is  $T \propto F^{1/4}$ , where F is the pump fluence<sup>31</sup>. Since  $\Delta R \propto T^2$ , we have  $\Delta R \propto \sqrt{F}$ . Therefore, close to the zero time delay where the disorderassisted process governs the relaxation, we expect square-root dependence of  $\Delta R/R$  on the pump fluence F. This is demonstrated in Fig. 3(b) where we plot  $\Delta R/R$  around zero time delay as a function of the pump fluence. The dashed curve is a square root fit exhibiting an excellent match to the data.

#### V. DYNAMICAL CHIRAL CHARGE PUMPING

Here we dicuss the pump-probe measurements in the presence of an applied static magnetic field. In Fig. 4(a), we plot  $\Delta R/R$  for B=0 T (black) and B=7 T (yellow). The two curves exhibit similar pump-probe responses close to the zero time delay, suggesting that the initial response for B=7 T is also related to pump-induced hot carriers. At longer time delays, when the carriers are expected to be cooled down to the quasiequilibrium temperature, the pump-probe trace at B=7 T exhibits a metastable positive response that does not fully recover within the 400 ps measurement range considered here. This suggests a process with a time constant of much greater than 1 ns but smaller than the repetition period of pulses (77 ns). The positive sign of the metastable signal suggests a pump-induced positive change in the conductivity, consistent with the nonlinear chiral charge pumping (3). Based on this picture, we interpret the metastable process to be the dynamical chiral pumping relaxation time  $\tau_{ch}$  which we estimate to be (1 ns  $\ll \tau_{\rm ch} < 77$  ns). This occurs in the N=0 chiral Landau level, which allows long-lived excitations due to the reduced phase space for scattering.

As presented later in this manuscript, the metastable response disappears when **E** and **B** are perpendicular to each another. In Fig. 4(b), we illustrate the expected pump-probe traces for fast hot carriers response (red), metastable chiral charge pumping response (blue), and the net response (green). As depicted in the right side of plot in Fig. 4(b), we define  $\Delta_1$ 

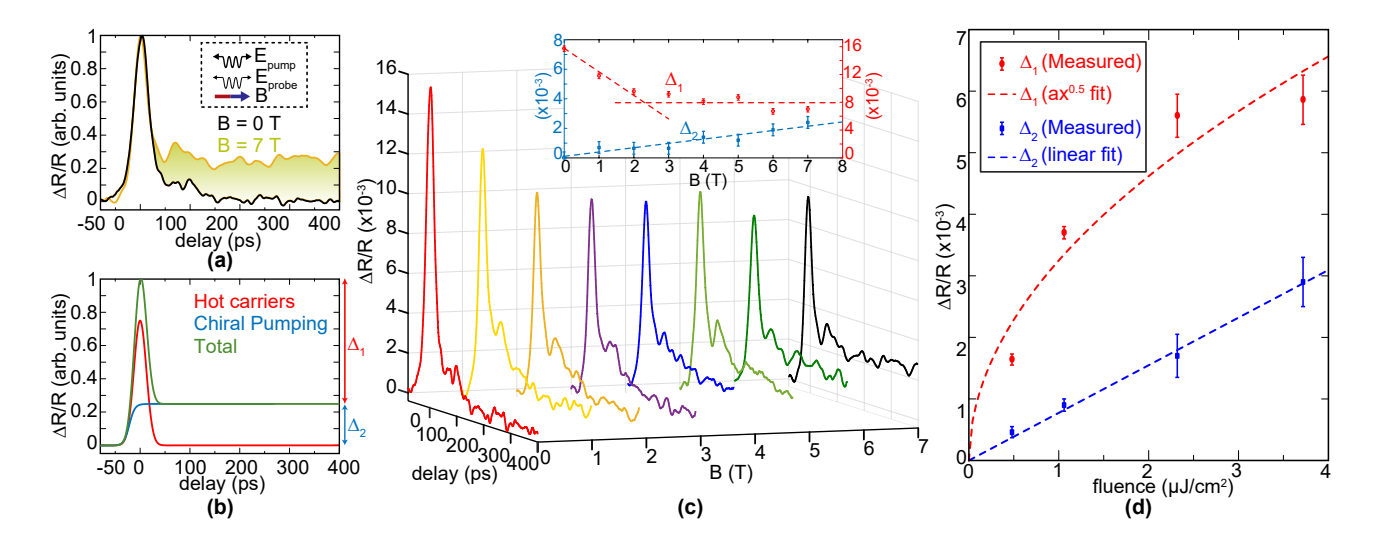


FIG. 4.  $E_{\text{pump}} \parallel E_{\text{probe}} \parallel B$  (varying B). (a) Pump-induced increase in probe reflection for B=0 T (black) and B=7 T (yellow) in arbitrary units as a function of pump-probe time delay. The peak around 60 ps is caused by a replica—the reflected pump pulse from the cryostat window. (b) Expected pump-probe traces for fast hot carriers effects (red), metastable chiral pumping (blue), and the net result (green). (c) Pump-probe trace for different static magnetic fields applied parallel to pump/probe polarization. The inset shows  $\Delta_1$  (red) and  $\Delta_2$  (blue) as a function of the applied magnetic field. (d)  $\Delta_1$  (red) and  $\Delta_2$  (blue) as a function of pump fluence. The red (blue) dashed lines are square-root (linear) fit.

as the size of the pump-probe signal at zero time delay, and  $\Delta_2$  as the size of the ultraslow signal. The long relaxation time of chiral charge pumping agrees well with theoretical estimations and is expected, given the large momentum transfer needed for carriers to transport between the Weyl nodes<sup>20</sup>. We note that the measured  $\tau_{\rm ch}$  is much larger than the values inferred indirectly from the negative magnetoresistance measurements<sup>12,13</sup>.

The observation of terahertz-excited  $\omega = (2\pi)3.4 \times 10^{12}$  rad/s chiral anomaly with a long relaxation time  $\omega \tau_{\rm ch} > 10^4$  holds promises for applications of Weyl semiemtals in quantum technology<sup>10</sup>. In order to further explore the observed metastable process and its relation to chiral charge pumping, we investigate the dependence of the metastable signal on the applied static magnetic field and the pump fluence.

### A. Magnetic Field Dependence

In Fig. 4(c), we show the measured pump-probe traces for variety of applied static magnetic fields from B=0 T to 7 T. The metastable response is present at all nonzero B values. Measurements at different magnetic fields exhibit similar fast pulsewidth-limited relaxation around zero time delay, followed by a slower tail with time constant of  $\approx$ 55 ps, similar to B=0 T case, except that the ones at non-zero magnetic field exhibit non-zero long-lived response, i.e.  $\Delta_2 \neq 0$  (see Fig. S4 in SM<sup>21</sup>). We note that the resolution of our pump-probe measurements is limited by the pulsewidth (30 ps), and thus any change in the relaxation time smaller than 30 ps are not measurable. As we increase B, the peak of the pump-probe response at zero time delay shrinks and goes to a constant value at higher magnetic fields, while the level of the metastable signal monotonically increases. We extract  $\Delta_1$  and  $\Delta_2$  from the

data in Fig. 4(b) and plot them as a function of the applied magnetic field in the inset. We note that this behavior is consistent with the origin of  $\Delta_1$  and  $\Delta_2$  to be related to hot carriers and nonlinear chiral charge pumping, respectively. As we increase the applied magnetic field from zero, carriers in the W2 Weyl node go to the quantum limit, so that for  $B \approx 2$  T, all W2 carriers are in LL0 (see Sec.VC in SM<sup>21</sup> for more details). Since the Drude weight of carriers in LL0 is independent of temperature<sup>36</sup>, the W2 carriers contribution to the initial hot carriers response diminishes as B is increased, and hence the decrease of  $\Delta_1$  at lower magnetic fields. As for  $\Delta_2(B)$ , according to (3), the pump-induced nonlinear magneto-optical conductivity increases with B causing the reflection change to increase. This predicts a linear dependence of  $\Delta_2$  on B, which is consistent with the experimental observations, as shown by the dashed blue curve in Fig. 4(c). In the Supplemental Materials<sup>21</sup>, Sec.VC, we carefully examine the contribution of carriers in different Weyl bands of W1 and W2 and the trivial carriers in TaAs to the observed pump-probe signals at zero and finite magnetic fields. We note that the conductivity measured in the presented pump-probe experiments is the nonlinear pump-induced change in the conductivity; the linear part of optical conductivity is normalized out in pump-probe traces. Fig. S1 in SM illustrates the charge pumping oscillations and its nonlinear pump-induced change that is being measured by pump-probe experiments. The pump fluence for all the presented data in Fig. 4 is  $3.7 \,\mu\text{J/cm}^2$ .

#### **B.** Pump Fluence Dependence

We investigate the dependence of  $\Delta_1$  and  $\Delta_2$  at B=7 T on the pump fluence. As shown in Fig. 4(d),  $\Delta_1$  is found to exhibit a sublinear dependence on the pump fluence. A

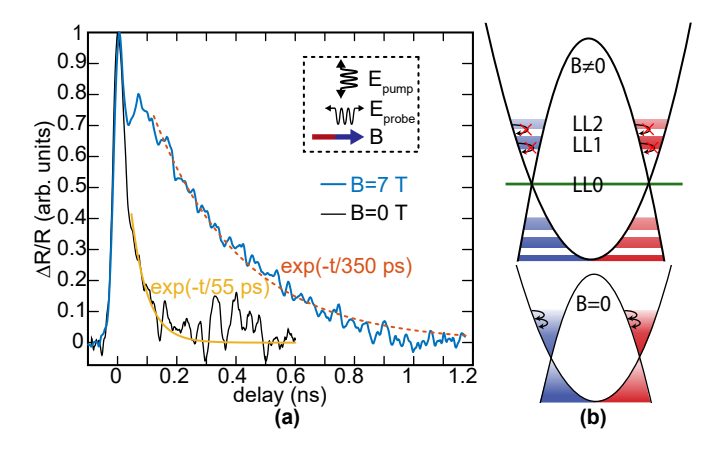


FIG. 5.  $E_{\text{pump}} \perp E_{\text{probe}} \parallel B$  (=7 T). (a) Relative pump-induced increase in probe reflection. (b) The phase space for phonon scattering of hot carriers in LLs (top panel) is strongly suppressed compared to zero magnetic field (bottom panel).

power-law fit to the measured  $\Delta_1$  vs pump fluence reveals a square-root-like dependence (dashed red curve in Fig. 4(d)), similar to the peak-vs-fluence dependence observed at B=0 T as shown in Fig. 3(b). The similarity to B=0 T measurements again points toward analogous hot carrier origin of  $\Delta_1$  at nonzero magnetic fields. On the other hand, as seen in Fig. 4(d),  $\Delta_2$  exhibits a perfectly linear dependence of the pump fluence. This suggests that the conductivity change is linear in the pump fluence and is in excellent agreement with the pump-induced change in the chiral pumping conductivity calculated in equation (3).

# VI. POLARIZATION DEPENDENCE: PERPENDICULAR FIELD GEOMETRY

To further confirm the interpretation of our results, we present the pump-probe measurement results with pump polarized perpendicular to the applied magnetic field, while keeping probe polarized parallel to the field. In this case, according to (3) and (4), we do not expect the pump pulse to excite a dynamical chiral current or change the chiral pumping conductivity, and therefore we do not expect to observe the metastable nonlinear chiral charge pumping signal. In Fig. 5(a), the blue curve is the measured pump-probe response at B = 7 T. First we note that the ultraslow metastable plateau observed for  $\mathbf{E}_{\text{pump}} \parallel \mathbf{B}$  is absent, supporting the nonlinear chiral charge pumping origin of the metastable signal as expected from (3). Therefore, as expected from (3) the observed metastable process for  $\mathbf{E}_{\text{pump}} \parallel \mathbf{B}$  attributed to pump-induced chiral charge pumping is absent for the case of  $\mathbf{E}_{\text{pump}} \perp \mathbf{B}$ .

Comparing the B=7 T result to B=0 T in Fig. 5(a), two main differences are noted: (i) the fast pulsewidth-limited relaxation process around the zero time delay is no longer present, and (ii) instead of the 55 ps tail, a slower process with the time constant of  $\approx 350$  ps extracted from the exponential fit (red dashed curve) appears. The two differences suggest that the pump-induced hot carriers relaxation processes

are strongly suppressed in the case of  $E_{pump} \perp B$ . Similar effects have been reported from pump-probe measurements on graphene in a magnetic field<sup>37</sup>. This effect is expected due to the strong reduction of phase space for carriers scattering in highly quantized Landau levels to scatter off the phonons, as illustrated in Fig. 5(b). In  $\mathbf{E}_{pump} \perp \mathbf{B}$  geometry, the tails of cyclotron resonances are excited and carriers are pumped to higher LLs. The relaxation of pump-induced hot electrons in W1 and W2 pockets to equilibrium involves inter-LL transitions, i.e. large energy and momentum scattering, that is hard to achieve with acoustic phonons+disorder in the phase-space limited LLs. We note that in our terahertz experiments, the optical phonons are not excited, since the photon energy of 14 meV and the energies associated with pump-induced carriers temperature rise (≈50 K) are below the optical phonon energies in TaAs<sup>38</sup>. The peak of pump-probe response exhibits an oscillatory behavior as a function of magnetic field due to the splitting of plasma edge in an applied field<sup>39</sup>. In the Supplemental Materials Sec.VI-VII<sup>21</sup>, we present more pump-probe data for  $\mathbf{E}_{pump} \perp \mathbf{B}$  case at different magnetic fields and pump fluences that all exhibit time dynamics similar to B = 7 T shown in Fig. 5(a).

#### VII. CONCLUSIONS

In the current manuscript, we introduce the concept of the dynamical chiral charge pumping and its optical control in a Weyl semimetal. We present the pump-probe results at zero magnetic field and conclude that the response is attributed to the pump-induced hot carriers in TaAs. We show the pump-probe measurement results at various magnetic fields applied parallel to pump/probe polarization, and for different pump fluences. Using a simple model for Weyl nodes<sup>40,41</sup> and nonlinear magneto-optical response<sup>42</sup>, we obtained the puminduced change in optical conductivity. Our experimental and theoretical results illustrate the ability to optically control the dynamical chiral charge pumping. While there is no static current produced by the pump pulse, it creates correlated excitations (or quasi-particles) in the opposing Weyl nodes that persist long after the pump pulse has passed. These quasiparticles alter the reflectivity of a subsequent weaker probe pulse in a measurable way. The lifetime associated with this nonlinearity is the dynamical chiral charge relaxation time, and is measured to be  $\tau_{ch} \gg 1$  ns. We further confirm our results by showing that for the case in which the pump polarization is perpendicular to the applied magnetic field, no long-lived response associated with nonlinear dynamical chiral charge pumping is observed. Our findings pave the way for future studies exploring optical control of topological transport phenomena in solids, and investigating long-lived chiral Weyl fermions for quantum optoelectronic applications.

#### ACKNOWLEDGEMENTS

M. K. acknowledges the support from the Sharif University of Technology under Grant No. G960208 and Iran Science

Elites Federation. Work at UCLA and UMD was supported by the U.S. Department of Energy (DOE), Office of Science,

Office of Basic Energy Sciences under Award Numbers DE-SC0011978 (UCLA), and DE-SC0005436 (UMD).

- \* mehdi.jadidi@columbia.edu
- † kargarian@physics.sharif.edu
- † hdrew@umd.edu
- <sup>1</sup> M. Mitrano, A. Cantaluppi, D. Nicoletti, S. Kaiser, A. Perucchi, S. Lupi, P. Di Pietro, D. Pontiroli, M. Riccò, S. R. Clark, D. Jaksch, and A. Cavalleri, Nature 530, 461 (2016).
- <sup>2</sup> Q. Ma, S.-Y. Xu, H. Shen, D. MacNeill, V. Fatemi, T.-R. Chang, A. M. Mier Valdivia, S. Wu, Z. Du, C.-H. Hsu, S. Fang, Q. D. Gibson, K. Watanabe, T. Taniguchi, R. J. Cava, E. Kaxiras, H.-Z. Lu, H. Lin, L. Fu, N. Gedik, and P. Jarillo-Herrero, Nature 565, 337 (2019).
- <sup>3</sup> E. J. Sie, C. M. Nyby, C. D. Pemmaraju, S. J. Park, X. Shen, J. Yang, M. C. Hoffmann, B. K. Ofori-Okai, R. Li, A. H. Reid, S. Weathersby, E. Mannebach, N. Finney, D. Rhodes, D. Chenet, A. Antony, L. Balicas, J. Hone, T. P. Devereaux, T. F. Heinz, X. Wang, and A. M. Lindenberg, Nature 565, 61 (2019).
- <sup>4</sup> A. A. Burkov and L. Balents, Physical Review Letters 107, 127205 (2011).
- <sup>5</sup> P. Hosur, S. A. Parameswaran, and A. Vishwanath, Physical Review Letters 108, 046602 (2012).
- <sup>6</sup> N. P. Armitage, E. J. Mele, and A. Vishwanath, Reviews of Modern Physics 90, 015001 (2018).
- <sup>7</sup> A. A. Zyuzin and A. A. Burkov, Physical Review B 86, 115133 (2012).
- <sup>8</sup> H. Nielsen and M. Ninomiya, Physics Letters B 130, 389 (1983).
- <sup>9</sup> P. Rivera, K. L. Seyler, H. Yu, J. R. Schaibley, J. Yan, D. G. Mandrus, W. Yao, and X. Xu, Science 351, 688 (2016).
- D. E. Kharzeev and Q. Li, arXiv:1903.07133 [cond-mat, physics:hep-th] (2019), arXiv:1903.07133 [cond-mat, physics:hep-th].
- <sup>11</sup> A. L. Levy, A. B. Sushkov, F. Liu, B. Shen, N. Ni, H. D. Drew, and G. S. Jenkins, Phys. Rev. B 101, 125102 (2020).
- <sup>12</sup> S. Liang, J. Lin, S. Kushwaha, J. Xing, N. Ni, R. J. Cava, and N. P. Ong, Physical Review X 8, 031002 (2018).
- <sup>13</sup> C.-L. Zhang, S.-Y. Xu, I. Belopolski, Z. Yuan, Z. Lin, B. Tong, G. Bian, N. Alidoust, C.-C. Lee, S.-M. Huang, T.-R. Chang, G. Chang, C.-H. Hsu, H.-T. Jeng, M. Neupane, D. S. Sanchez, H. Zheng, J. Wang, H. Lin, C. Zhang, H.-Z. Lu, S.-Q. Shen, T. Neupert, M. Zahid Hasan, and S. Jia, Nature Communications 7, 10735 (2016).
- <sup>14</sup> L. Wu, S. Patankar, T. Morimoto, N. L. Nair, E. Thewalt, A. Little, J. G. Analytis, J. E. Moore, and J. Orenstein, Nature Physics 13, 350 (2017).
- <sup>15</sup> Q. Ma, S.-Y. Xu, C.-K. Chan, C.-L. Zhang, G. Chang, Y. Lin, W. Xie, T. Palacios, H. Lin, S. Jia, P. A. Lee, P. Jarillo-Herrero, and N. Gedik, Nature Physics 13, 842 (2017).
- <sup>16</sup> G. B. Osterhoudt, L. K. Diebel, M. J. Gray, X. Yang, J. Stanco, X. Huang, B. Shen, N. Ni, P. J. Moll, Y. Ran, and K. S. Burch, Nature Materials 18, 471 (2019).
- <sup>17</sup> J. Ma, Q. Gu, Y. Liu, J. Lai, P. Yu, X. Zhuo, Z. Liu, J.-H. Chen, J. Feng, and D. Sun, Nature Materials 18, 476 (2019).
- <sup>18</sup> X. Huang, L. Zhao, Y. Long, P. Wang, D. Chen, Z. Yang, H. Liang, M. Xue, H. Weng, Z. Fang, X. Dai, and G. Chen, Physical Review X 5, 031023 (2015).
- F. Arnold, C. Shekhar, S.-C. Wu, Y. Sun, R. D. dos Reis, N. Kumar, M. Naumann, M. O. Ajeesh, M. Schmidt, A. G. Grushin, J. H. Bardarson, M. Baenitz, D. Sokolov, H. Borrmann, M. Nick-

- las, C. Felser, E. Hassinger, and B. Yan, Nature Communications 7, 11615 (2016).
- <sup>20</sup> S. A. Parameswaran, T. Grover, D. A. Abanin, D. A. Pesin, and A. Vishwanath, Physical Review X 4, 031035 (2014).
- <sup>21</sup> See Supplemental Materials.
- <sup>22</sup> S.-M. Huang, S.-Y. Xu, I. Belopolski, C.-C. Lee, G. Chang, B. Wang, N. Alidoust, G. Bian, M. Neupane, C. Zhang, S. Jia, A. Bansil, H. Lin, and M. Z. Hasan, Nature Communications 6, 7373 (2015).
- <sup>23</sup> F. Arnold, M. Naumann, S.-C. Wu, Y. Sun, M. Schmidt, H. Borrmann, C. Felser, B. Yan, and E. Hassinger, *Physical Review Letters* 117, 146401 (2016).
- <sup>24</sup> D. T. Son and B. Z. Spivak, Physical Review B 88, 104412 (2013).
- <sup>25</sup> F. de Juan, A. G. Grushin, T. Morimoto, and J. E. Moore, Nature Communications 8, 15995 (2017).
- <sup>26</sup> S.-Y. Xu, I. Belopolski, N. Alidoust, M. Neupane, G. Bian, C. Zhang, R. Sankar, G. Chang, Z. Yuan, C.-C. Lee, S.-M. Huang, H. Zheng, J. Ma, D. S. Sanchez, B. Wang, A. Bansil, F. Chou, P. P. Shibayev, H. Lin, S. Jia, and M. Z. Hasan, Science 349, 613 (2015).
- <sup>27</sup> B. Q. Lv, H. M. Weng, B. B. Fu, X. P. Wang, H. Miao, J. Ma, P. Richard, X. C. Huang, L. X. Zhao, G. F. Chen, Z. Fang, X. Dai, T. Qian, and H. Ding, Physical Review X 5 (2015), 10.1103/Phys-RevX.5.031013.
- <sup>28</sup> C.-C. Lee, S.-Y. Xu, S.-M. Huang, D. S. Sanchez, I. Belopolski, G. Chang, G. Bian, N. Alidoust, H. Zheng, M. Neupane, *et al.*, Physical Review B **92**, 235104 (2015).
- <sup>29</sup> B. Xu, Y. M. Dai, L. X. Zhao, K. Wang, R. Yang, W. Zhang, J. Y. Liu, H. Xiao, G. F. Chen, A. J. Taylor, D. A. Yarotski, R. P. Prasankumar, and X. G. Qiu, Physical Review B 93, 121110 (2016).
- <sup>30</sup> G. S. Jenkins, C. Lane, B. Barbiellini, A. B. Sushkov, R. L. Carey, F. Liu, J. W. Krizan, S. K. Kushwaha, Q. Gibson, T.-R. Chang, H.-T. Jeng, H. Lin, R. J. Cava, A. Bansil, and H. D. Drew, Physical Review B 94, 085121 (2016).
- <sup>31</sup> R. Lundgren and G. A. Fiete, Physical Review B **92**, 125139 (2015).
- <sup>32</sup> J. C. Song, M. Y. Reizer, and L. S. Levitov, Physical Review Letters 109, 106602 (2012).
- <sup>33</sup> M. M. Jadidi, R. J. Suess, C. Tan, X. Cai, K. Watanabe, T. Taniguchi, A. B. Sushkov, M. Mittendorff, J. Hone, H. D. Drew, M. S. Fuhrer, and T. E. Murphy, Physical Review Letters 117, 257401 (2016).
- <sup>34</sup> M. W. Graham, S.-F. Shi, D. C. Ralph, J. Park, and P. L. McEuen, Nature Physics 9, 103 (2013).
- M. M. Jadidi, J. C. Konig-Otto, S. Winnerl, A. B. Sushkov, H. D. Drew, T. E. Murphy, and M. Mittendorff, Nano Letters 16, 2734 (2016).
- <sup>36</sup> J. Gooth, A. C. Niemann, T. Meng, A. G. Grushin, K. Landsteiner, B. Gotsmann, F. Menges, M. Schmidt, C. Shekhar, V. Süß, R. Hühne, B. Rellinghaus, C. Felser, B. Yan, and K. Nielsch, Nature 547, 324 (2017).
- <sup>37</sup> M. Mittendorff, M. Orlita, M. Potemski, C. Berger, W. A. de Heer, H. Schneider, M. Helm, and S. Winnerl, New Journal of Physics 16, 123021 (2014).
- <sup>38</sup> H. Liu, P. Richard, Z. Song, L. Zhao, Z. Fang, G.-F. Chen, and H. Ding, Physical Review B **92**, 064302 (2015).

- $^{\rm 39}\,$  J. G. Mavroides, Optical properties of solids. North Holland, Amsterdam (1972).
- <sup>40</sup> M. Kargarian, M. Randeria, and N. Trivedi, Scientific Reports 5, 12683 (2015).
- <sup>41</sup> P. Goswami, J. H. Pixley, and S. Das Sarma, Physical Review B
- 92, 075205 (2015).
  T. Morimoto, S. Zhong, J. Orenstein, and J. E. Moore, Physical Review B 94 (2016), 10.1103/PhysRevB.94.245121.